Study on Aerodynamic Performance of Morphing Hypersonic Vehicle in Wide-Speed Range

LUO Shibin, YUE Hang, LIU Jun, SONG Jiawen, CAO Wenbin*

Research Institute of Aerospace Technology, Central South University, Changsha 410083, P.R. China

(Received 11 March 2023; revised 20 December 2023; accepted 20 March 2024)

Abstract: Wide-speed range flight is a critical design objective and development direction for hypersonic vehicles. However, the complex environmental changes pose design conflicts for fixed-configuration vehicles under different flight conditions. Hypersonic morphing vehicles can adapt to various flight conditions and meet performance requirements by presenting different configurations. This paper introduces numerical simulations to investigate the aerodynamic characteristics of a foldable-wing vehicle, and focuses on the lift-to-drag ratio, longitudinal static stability, and directional static stability of the aerodynamic configuration in different wing folding states at various flight altitudes and Mach numbers. The impact of varying wing folding angles (0°, 45°, 90°) on the aerodynamic performance are compared. The results indicate that across the entire range of speeds studied (Ma=0—5), the smaller wing folding angles result in the higher lift coefficients, drag coefficients, and lift-to-drag ratios. The wing folding angle of 0° exhibits the highest lift-to-drag ratio. In terms of longitudinal stability, the configuration with a smaller folding angle has better longitudinal stability. As the Mach number increases, the differences in longitudinal stability between different folding angles initially decrease and then increase. The static stability margins change from 1∶0.95∶0.84 to 1∶0.98∶0.88, then to 1∶0.89∶0.79. In addition, configurations with larger wing folding angles exhibit better directional stability. All three wing folding configurations are directionally stable during the low-speed flight phase. As the Mach number increases, the 0° and 45° folding angles gradually become directionally unstable.

Key words: wide-speed range; morphing vehicle; folding wing; aerodynamic performance; hypersonic vehicle

CLC number: TN925 **Document code:** A **Article ID:** 1005-1120(2024)02-0184-18

0 Introduction

The hypersonic vehicle equipped with a combined cycle engine can have horizontal takeoff and landing, reusability, and high-speed cruising in near space. This type of vehicle offers substantial advantages in terms of survivability and combat capabilities due to its high speed and altitude. It has the potential to overcome existing defense systems and can fulfill various mission requirements such as surveillance, strike operations, and transportation between space and Earth. Consequently, both domestic and international researchers have shown great interest in this technology[1].

Hypersonic vehicles have a broad range of altitude capabilities, operate at high speeds, and incorporate innovative engine systems. However, the environmental changes experienced during flight pose significant challenges in the aerodynamic configuration design of hypersonic vehicles. These challenges primarily manifest in the following aspect[2].

(1) Lift-to-drag ratio design requirements

When designing a vehicle capable of wide-speed range flight, the first challenge is that different types of vehicles have different aerodynamic configuration characteristics. The aerodynamic configuration design usually tends to meet the design requirements for the hypersonic flight phase. In the hypersonic phase, an aerodynamic configuration with a high slenderness ratio, large sweep angle, and

*Corresponding author, E-mail address: liu.jun@csu.edu.cn.

How to cite this article: LUO Shibin, YUE Hang, LIU Jun, et al. Study on aerodynamic performance of morphing hypersonic vehicle in wide-speed range[J]. Transactions of Nanjing University of Aeronautics and Astronautics, 2024, 41(2): 184-201.
http://dx.doi.org/10.16356/j.1005-1120.2024.02.005

small aspect ratio performs better. However, these design characteristics may result in insufficient lift during takeoff and landing.

Additionally, selecting airfoil profiles and using trailing edge flaps or other components can effectively delay flow separation, thereby increasing lift. However, as the flight transitions to transonic and higher speeds, the lift-to-drag ratio is predominantly influenced by the pressure difference between the compression on the windward side and the expansion on the leeward side of the incoming airflow rather than by a single component. Changes in the lift mechanism and the occurrence of shockwaves directly impact the vehicle's aerodynamic configuration design. A significant swept-back wing can lower the critical Mach number, while a small aspect ratio design helps reduce wave drag. Furthermore, increasing the integration of blended wing-body design can minimize interference caused by wave systems. Considering the need to address external environmental changes and adapt the lift mechanism, designing for a high lift-to-drag ratio throughout the entire wide-speed range flight poses a substantial challenge.

(2) Longitudinal stability requirements

In transonic flight, shock waves affect the lift-to-drag ratio and introduce challenges to the design of the aerodynamic configuration by influencing stability and control characteristics. The longitudinal stability of the vehicle is assessed through the static stability margin, which represents the relative position of the aerodynamic center in relation to the center of mass. This margin determines the direction of the resulting moment caused by external disturbances acting upon the vehicle. The aerodynamic center experiences significant shifts as the vehicle transitions from subsonic to transonic, supersonic, and hypersonic speeds. Initially, it shifts backward and then forward. These shifts in the aerodynamic center have a considerable impact on the longitudinal stability of the vehicle, thereby presenting another difficulty in the design of the aerodynamic configuration for wide-speed hypersonic vehicles.

(3) Lateral and directional stability requirements

The aerodynamic design of a hypersonic vehicle typically incorporates a small aspect ratio, which helps optimize its performance at high speeds and reduce wave drag. However, the disadvantage of this design is that the vehicle has poor heading and lateral stability. As the Mach number increases, the lateral and directional stability diminishes significantly. Moreover, in high-altitude and high Mach number flight conditions, the efficiency of control surfaces is compromised, making it more difficult to achieve proper trim and affecting the lift-to-drag ratio. Therefore, to address the conflicting requirements of lateral and directional stability across a wide range of speeds, it becomes necessary to introduce novel supplementary control surfaces in the design of wide-speed range vehicles. These additional control surfaces help resolve the stability design contradiction while maintaining effective control characteristics throughout the flight envelope.

Many traditional hypersonic vehicles utilize aerodynamic configurations like the revolution body, wave-rider body, and lifting body. These configurations primarily focus on optimizing aerodynamic performance during hypersonic flight and usually struggle to meet the aerodynamic requirements at subsonic, transonic, and supersonic speeds—deviation from the design point results in a sharp deterioration in aerodynamic performance. Therefore, morphing aerodynamic configuration design is crucial for the vehicle to adapt to flight conditions within a wide speed range. Vehicles have the potential to maintain excellent flight performance throughout the entire flight process by appropriately adjusting their aerodynamic configuration.

To adapt to different external environments and changes in flight states, adjusting the aerodynamic configuration of a vehicle is not a new concept. One example is the F-111 fighter developed by General Dynamics in 1965, which incorporates a variable swept-back wing[3]. This design features an extensive swept-back configuration to reduce drag during supersonic flight and a smaller swept-back configuration for subsonic flight. The variation of the wing sweep angle can also change the wing area, providing sufficient lift for the vehicle during the

takeoff and landing phases.

Various morphing configuration schemes have been proposed to achieve a wide range of flight capabilities. These morphing configurations can typically be categorized into four groups: Wing deformation, fuselage deformation, dynamic system deformation, and hybrid deformation based on the deformed part. Further classification can be done based on characteristics like the deformation range and the deformation method. In addition to the design of aerodynamic configuration schemes, the effect of configuration deformation on aerodynamic performance under different flight conditions is also an important research content. Among these categories, large-scale wing deformation, such as variable span length, variable swept-back, and wing folding, has garnered substantial interest from researchers worldwide.

Ref.[4] proposed a wide-speed range hypersonic vehicle with wing rotational deformation, employing the following morphing scheme: During subsonic flight, the wings rotate outwards from the fuselage, thereby reducing the wing swept-back angle and enhancing the vehicle's aerodynamic performance at subsonic speeds. In the transonic and supersonic flight states, the wings rotate towards the interior of the fuselage, and the swept-back angle is increased to reduce wave drag. The wings are retracted into the fuselage for hypersonic speeds, transforming the vehicle into a hypersonic aerodynamic configuration. Research results indicate that increasing the aspect ratio of the configuration yields more lift at lower Mach numbers while gradually increasing the swept-back angle reduces drag as the flight speed increases.

Ref.[5] adopted a morphing scheme involving flexible canards to balance subsonic takeoff and hypersonic cruise performance. The scheme selected the blended wing body configuration with a large sweep angle delta wing. Meanwhile, the extension of the canards provides supplemental lift during subsonic conditions, effectively improving takeoff and landing performance.

Ref.[6] investigated two types of wing swept-back configurations, namely "rotating swept-back" and "shearing swept-back". The wingtip's direction and airfoil after deformation are different. The aerodynamic performance of these configurations is then evaluated and compared.

Previous research has focused on exploring innovative deformation modes, evaluating aerodynamic performance, and optimizing configurations[7]. However, the existing studies on the aerodynamic performance of morphing vehicles have mainly concentrated on the lift and drag characteristics while neglecting other crucial indicators such as stability and control characteristics. Furthermore, relatively less attention has been paid to the aerodynamic characteristics during the morphing process.

To further understand the performance characteristics of different configurations of hypersonic morphing vehicles in the wide-speed range, this paper adopts a numerical simulation method to systematically study the aerodynamic performance and static stability characteristics of a morphing hypersonic vehicle in subsonic, transonic, supersonic, and hypersonic states for the first time[8]. It analyzes the flow mechanism that leads to these characteristics, expecting to provide a reference for the design of wide-speed range aerodynamic configuration.

1 Aerodynamic Configuration Design

1.1 Configuration scheme

Based on the existing research, many configuration schemes have been proposed for achieving wide-speed range flight in supersonic and hypersonic vehicles. The U.S. XB-70[9] supersonic vehicles exemplify one prominent aerodynamic configuration. The configuration features a large slenderness ratio fuselage, a delta wing with a significant swept-back angle, double vertical fins, and a canard positioned at the forward section of the fuselage. The canard serves dual purposes as both a lift and control surface, enhancing lift during takeoff and landing while improving control and stability characteristics in the pitch channel. The engine is located in the fuselage's midsection, allowing the vehicle's frontal body to compress the incoming flow. In addition, wingtips

can be folded downward at different speed conditions. By adjusting the wing folding angle, the aerodynamic configuration of the vehicle can adapt to different flight environments.

The U. S. SR-71[10], renowned for its maximum flight Mach number of 3.35, incorporates various aerodynamic features to achieve outstanding performance. It incorporates a large slenderness ratio fuselage, a delta wing with a substantial swept-back angle, and a blended-wing-body configuration. These design choices allow it to possess subsonic and supersonic vehicle configuration characteristics simultaneously. The engine is in the middle of the wing, maintaining a certain distance from the fuselage. This configuration reduces aerodynamic interference between the fuselage and the engine, thereby improving the overall aerodynamic efficiency of the fuselage.

Furthermore, the wing design of the SR-71 adopts a thin airfoil and incorporates strake wings. This design serves multiple purposes. Firstly, it provides vortex lift at subsonic speeds, addressing the challenge of insufficient lift during takeoff and landing for supersonic vehicle configurations. Secondly, the strake wing increases the sweep angle of the wing's leading edge, raising the critical Mach number and effectively reducing wave drag[11]. These aerodynamic features contribute to the SR-71's exceptional performance capabilities.

An aerodynamic configuration scheme of the morphing vehicle is proposed based on successful aerodynamic configuration cases of existing supersonic vehicles. The design process considers the application background of wide-speed range flight, combining the performance advantages of different shapes under different flight conditions by wing folding. This allows the vehicle to possess the external characteristics of both high-speed and low-speed vehicles and adjust aerodynamic performance by wing folding[12].

The vehicle features a large swept delta wing and a double vertical tail configuration regarding the fuselage. The fuselage is seamlessly integrated with the strake and large swept delta wings, forming a blended wing body. The wings are designed with a foldable outer wing component, allowing for adjusting the folding angle θ based on external conditions and mission requirements. The wing folding angle impacts key external parameters such as wing span, wing projected area, and aspect ratio. Fig.1 illustrates the aerodynamic configuration of the vehicle with various wing folding angles(θ=0°, 45°, 90°).

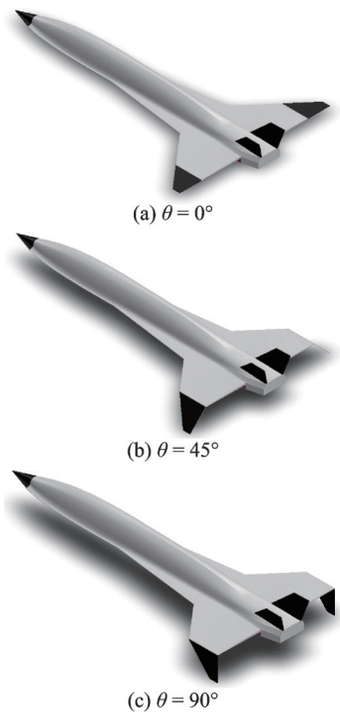

Fig.1 Schematic diagrams of different wing folding angles of vehicle

Table 1 summarizes the main shape parameters of the hypersonic vehicle and the variation range of relevant parameters during wing folding.

Table 1 Shape parameters of folding wing vehicle

Parameter	Numerical value
Fuselage length/m	11.8
Wing span/m	4.9—6.9
Fuselage height/m	0.88
Wing area range/m^2	4.31—4.72—5.06
Sweep angle of strake wing/(°)	83
Sweep angle of main wing/(°)	41
Aspect ratio range	0.7—1.5
Leading edge passivation radius/mm	10

1.2 Mesh generation

For flow simulation in this study, a hybrid mesh is employed. During the mesh generation pro-

cess, the far field boundary is set at 15 times the length of the fuselage, and the boundary layer mesh near the wall undergoes refinement. The first layer mesh has a height of 0.005 mm, with a growth rate of 1.05 in the normal direction. Prismatic cells are used for meshing around the wall, while tetrahedral cells are used for far-field meshes away from the wall. The total volume mesh consists of approximately 17 million cells. Figs.2—4 show the division of surface, volume, and symmetrical plane mesh, respectively.

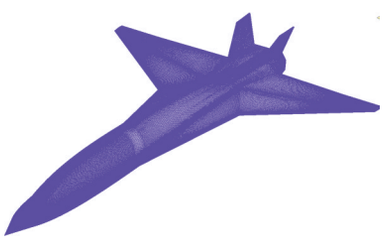

Fig.2 Vehicle surface meshing of vehicle

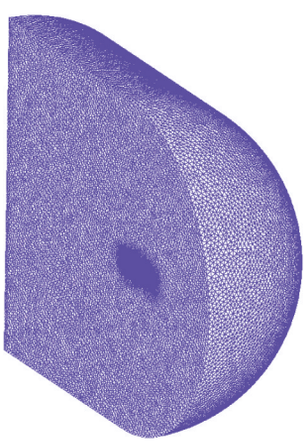

Fig.3 Volume mesh of vehicle

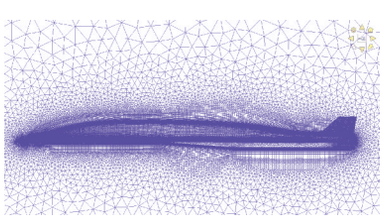

Fig.4 Mesh at symmetry plane and wall

2 Numerical Simulation Method Verification

This study utilizes an efficient in-house code for computational fluid dynamics (CFD) numerical simulation. The code is based on GPU acceleration and solves the Reynolds-averaged Navier-Stokes equations. It employs a finite-volume method, the k-ω SST turbulence model, and the AUSMPW+ upwind scheme[13-14]. An aerospace vehicle model from the literature is selected to validate the effectiveness and accuracy of the numerical method in simulating hypersonic outflow fields. The numerical simulation results are compared and analyzed with wind tunnel test data, demonstrating the code's reliability. Fig.5 illustrates the wind tunnel test model of the aerospace plane[15].

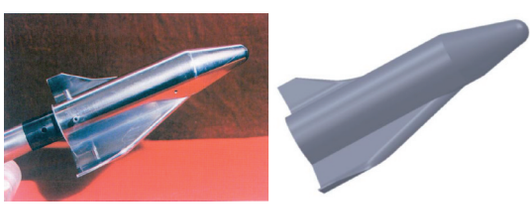

Fig.5 Wind tunnel test model and geometry model

Fig.6(a) shows that the lift coefficient C_L agrees well with the experimental data. In Fig.6 (b), the drag coefficient C_D also displays satisfactory agreement with the experimental data at small angles of attack α. Still, it exhibits slightly higher values than the experimental data at larger angles of attack. According to subsequent studies on static stability, Fig.6(c) compares the pitch moment coefficient C_{mz}. Nevertheless, the overall accuracy remains reasonable, confirming the numerical method's suitability for this research.

Fig.7 compares the numerical simulation results and the experimental schlieren diagram at an angle of attack of 10°. The numerical calculations align well with the wind tunnel test results.

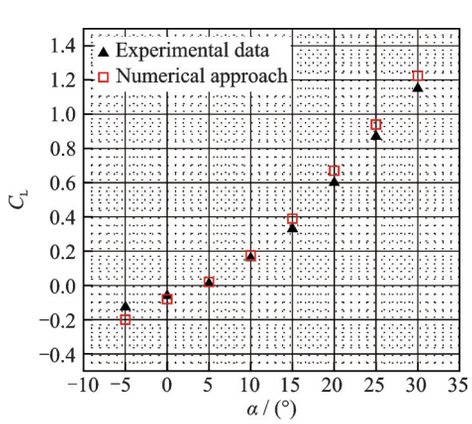

(a) Lift coefficient

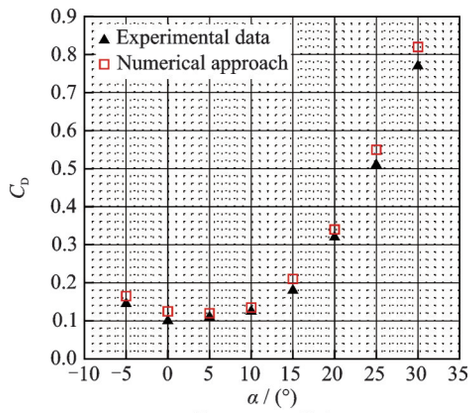

(b) Drag coefficient

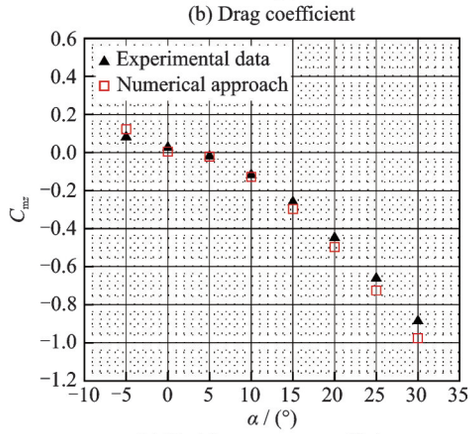

(c) Pitching moment coefficient

Fig.6 Comparison of calculated and experimental data

(a) Experimental result

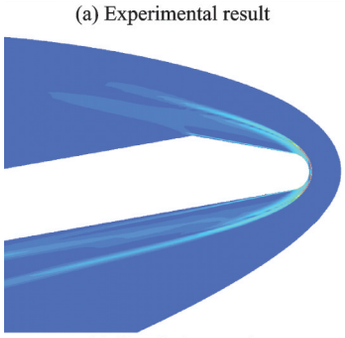

(b) Simulation result

Fig.7 Comparison of density gradient between simulation and experiment

Based on the analysis above, it can be concluded that the numerical method employed in this study effectively captures the external flow field characteristics of hypersonic vehicles. The numerical simulation results exhibit a high level of confidence and reliability.

3 Aerodynamic Characteristic Analysis

3.1 Numerical simulation study

To study the aerodynamic characteristics of the folding wing vehicle at different flight speeds, this research considers four flight conditions: Subsonic, transonic, supersonic, and hypersonic. These conditions encompass a range of altitudes from 0 to 24 km and Mach numbers from 0 to 5, covering the typical conditions and flight states encountered by comprehensive speed range vehicles. Furthermore, to analyze various modes during the wing folding process, three wing folding angles (0°, 45°, and 90°) are selected for numerical simulation, encompassing the start, stop, and intermediate stages of morphing. In addition to changes in flight altitude and Mach number, the variation range of the angle of attack and sideslip angle is 0°—8° with an interval of 2°. The performance parameters analyzed and studied are lift coefficient, drag coefficient, and static stability. Detailed operating conditions are summarized in Table 2.

Table 2 Calculation conditions for folding wing vehicle

θ/(°)	H/km	Ma	α/(°)	β/(°)
0/45/90	0	0.3	0/2/4/6/8	0/2/4/6/8
0/45/90	5	0.8	0/2/4/6/8	0/2/4/6/8
0/45/90	15	2	0/2/4/6/8	0/2/4/6/8
0/45/90	24	5	0/2/4/6/8	0/2/4/6/8

3.2 Subsonic-speed aerodynamic characteristics analysis

Numerical simulations are conducted in the subsonic condition of Ma 0.3 to explore how the vehicle's lift, drag, longitudinal stability, and directional stability vary with the angle of attack and sideslip angle. Subsequently, the numerical results are utilized to compare the performance across different wing folding angle configurations.

According to Fig.8, the lift coefficient C_L and drag coefficient C_D trend with respect to the angle of

attack are consistent for different folding angles θ. When calculating these coefficients of different wing folding states, the reference area is the same with the value of 1 m^2. Comparing different curves, it can be observed that as the wing folding angle of the vehicle decreases, the lift and drag coefficients increase[16]. The difference in lift coefficient is more significant than the drag coefficient. Moreover, a larger wing folding angle leads to a smaller lift-to-drag ratio L/D. The lift-to-drag ratio initially increases and then decreases with the angle of attack, reaching its maximum value around 4° angle of attack without sideslip. Within the range of 4° to 8° angle of attack, the lift-to-drag ratio decreases rapidly for the configuration with 0° folding angle due to a rapid increase in drag within this range. The difference in lift-to-drag ratio gradually narrows compared to the setup with a 45° folding angle[17].

Fig.9 shows the streamline distribution of the axial section of the wing for three different wing folding angles θ. The streamlines' color also reflects the pressure distribution in the flow field. By comparing the diagrams, it can be observed that the wing folding angle significantly impacts the vortex region on the upper surface within the outer wing section. The gradually rising outer wing obstructs the airflow underneath the wing from flowing over the wingtip towards the low-pressure region on the upper surface. The low-pressure airflow near the wingtip continuously moves downwards towards the

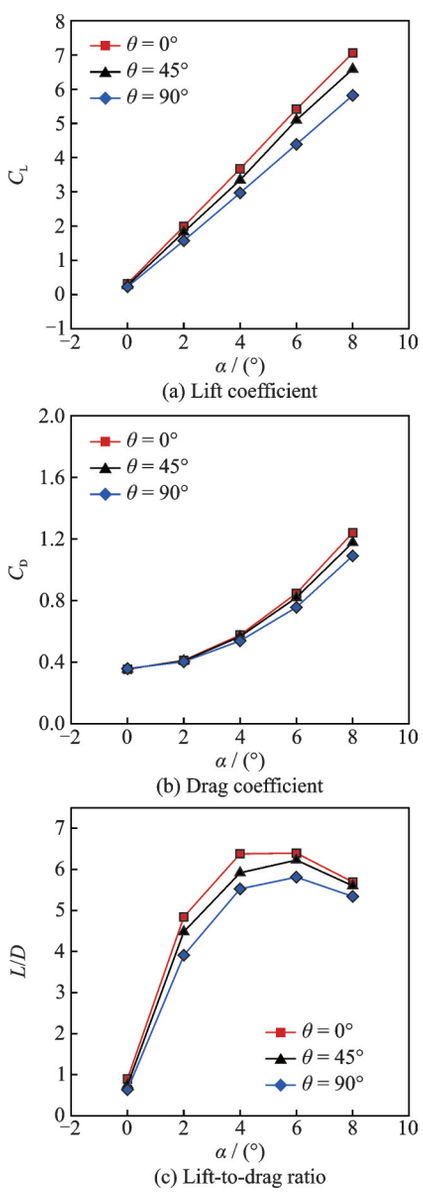

Fig.8 Variation of lift-drag characteristics with angle of attack (H = 0 km, Ma = 0.3, β = 0°)

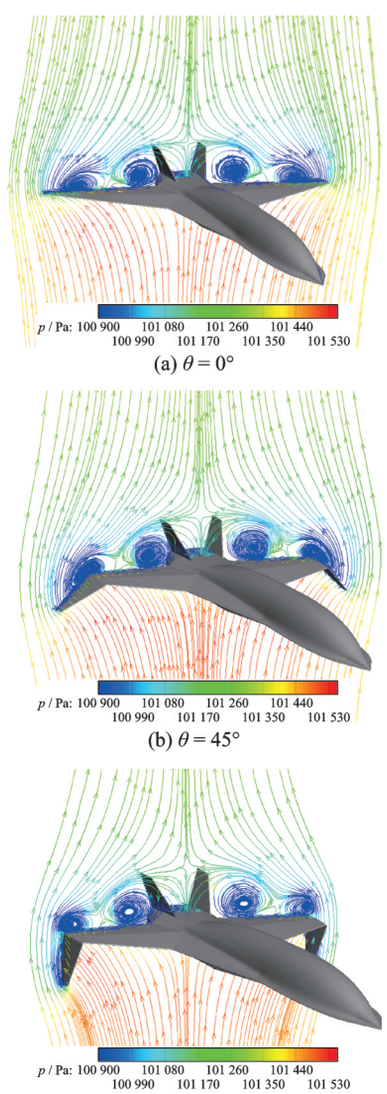

Fig.9 Streamline diagrams at x=10.9 m slice (Ma=0.3, α=8°)

side with wing folding. As a result, the extent and intensity of the vortex region on the wing's upper surface decrease as the folding angle increases. The pressure difference between the upper and lower surfaces also gradually decreases, leading to a loss of lift.

Before researching a vehicle's stability, it is necessary to define the relevant reference values, coordinate systems, and directions. The moment coefficient is referenced to a point at (7.0, −0.008, 0), assumed to be the center of mass (with a mean value of $\bar{x}_{cg}=0.6$). Additionally, the positive direction for the pitching moment is defined as upward. The subsequent research on the vehicle's stability is based on the same definitions, which will not be repeated.

Based on the curve of the pitching moment coefficient C_{mz}, it can be observed that in the subsonic speed state ($Ma=0.3$), as the angle of attack increases, the downward moment of all three wing folding angle configurations increases ($M_z^{\alpha}<0$). This indicates that vehicles in different wing folding states are all longitudinally statically stable. Under the subsonic speed condition, the primary lift generation is attributed to the wing. The longitudinal center of pressure typically lies close to the wing, generally at the vehicle's rear body. A larger folding angle corresponds to a smaller wing area and span, resulting in a decreased lift coefficient. Consequently, the aerodynamic contribution from the wing becomes relatively smaller. The pressure center coefficient X_{cp} and the aerodynamic center coefficient X_{ac} move forward, approaching the center of mass. Therefore, by considering the slope of the pitch moment curve and the static stability margin presented in Fig.10 and Fig.11, it is evident that configurations with smaller folding angles exhibit better longitudinal stability in subsonic conditions.

From Fig.12, it can be observed that under Ma=0.3 conditions, the yawing moment coefficient C_{my} of the vehicle increases with the increase of sideslip angle for three wing folding configurations. All three configurations exhibit static stability in yawing motion. Under the effect of lateral airflow, the downward folded wing generates a force in the same direction as yawing, creating an additional yawing restoring moment relative to the center of mass. As the folding angle increases, the effective area of the wing relative to the lateral airflow also increases, resulting in an increased restoring moment. Therefore, a larger folding angle of the wing corresponds to better yawing stability. The difference in slope of the yawing moment curve concerning the sideslip angle also indicates that larger folding angles result in a faster increase in the yawing moment with the side-

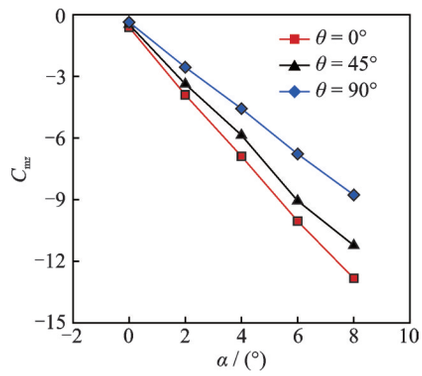

Fig.10 Pitching moment coefficient (H = 0 km, Ma = 0.3, β = 0°)

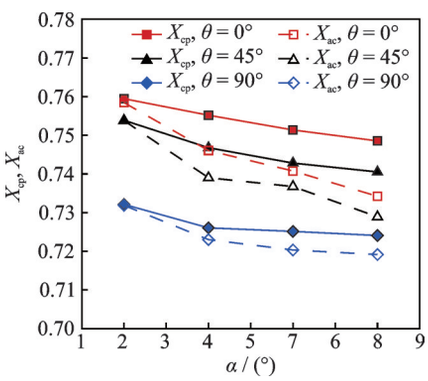

Fig.11 Coefficients of pressure center and aerodynamic center (H = 0 km, Ma = 0.3, β = 0°)

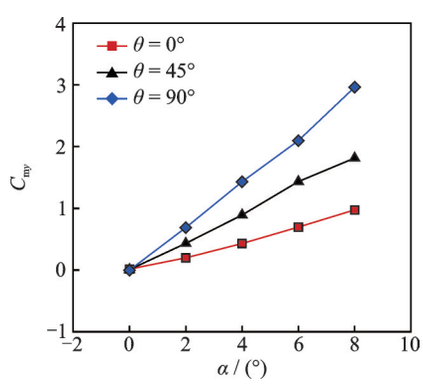

Fig.12 Yawing moment coefficient (H = 0 km, Ma = 0.3, β = 0°)

slip angle, indicating better directional stability.

3.3 Transonic-speed aerodynamic characteristics analysis

Under transonic conditions, the aerodynamic characteristics of the morphing vehicle are similar to those observed under subsonic conditions. The lift and drag coefficients are higher, but their variation trends with angle of attack are consistent. Different folding angle configurations also exhibit differences in lift and drag characteristics. Fig.13 illustrates the lift and drag characteristics of the vehicle. The smaller the folding angle, the higher the lift coefficient, drag coefficient, and lift-to-drag ratio.

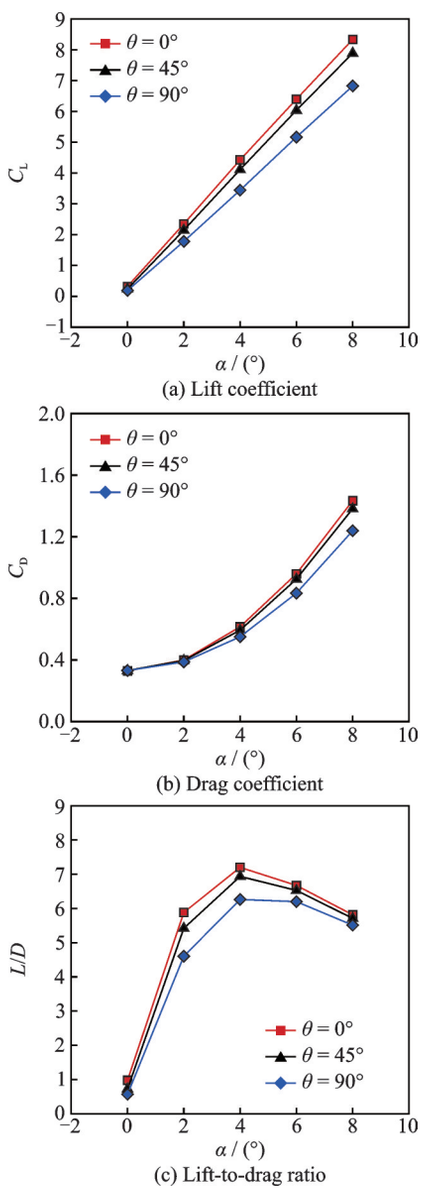

Fig.13 Variation of lift and drag characteristics with angle of attack (H = 5 km, Ma = 0.8, β = 0°)

Fig.14 shows the streamlines distribution of the axial section of the wing for three different wing folding angles. A distinct vortex region is formed at the transition area between the wing and the fuselage on the vehicle's upper surface. The pressure contour lines also reflect the vortex structure, resulting in two noticeable low-pressure regions on the upper surface. The pressure difference between the upper and lower surfaces generates lift. Compared to the subsonic state, the wing folding consistently affects the vortex region (low-pressure region). The low-pressure region on the upper surface of the outer wing narrows and approaches the wall, gradually tilting downwards along the upper surface. The in-

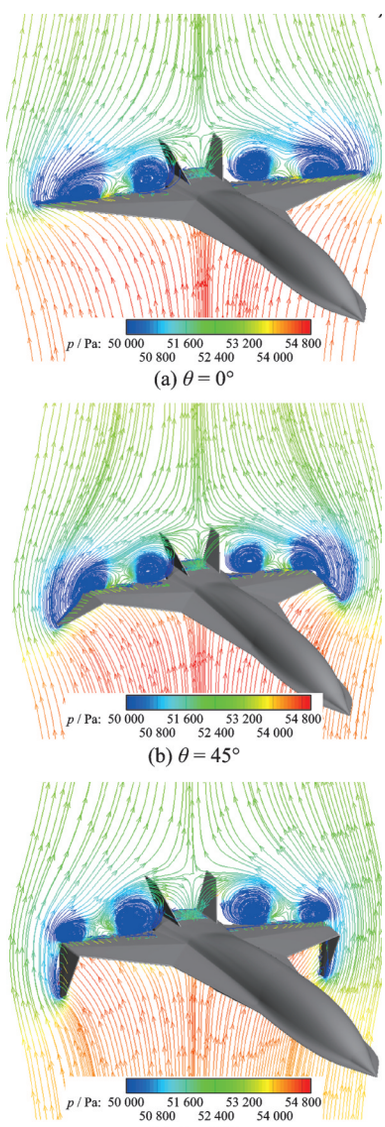

Fig.14 Streamline diagram at x = 10.9 m slice (Ma = 0.8, α = 8°)

tensity and range of the vortex region decrease, leading to a loss of lift.

As the flight speed increases from subsonic to transonic, the lift coefficient increases, and the lift loss caused by wing folding also increases, resulting in a more significant difference in lift coefficient between the 90° folding angle and the other two folding angle configurations. While experiencing lift loss, wing folding also reduces the induced drag of the vehicle. The drag coefficients of the 0° and 45° folding angle configurations are similar but significantly more extensive than that of the 90° folding angle configuration. Considering the combined effect of lift coefficient and drag coefficient, the loss of lift caused by outer wing folding is greater than the reduction of drag. Under the subsonic condition (Ma=0.8), the vehicle's lift-to-drag ratio decreases as the wing folding angle increases.

From the curve of the pitching moment coefficient with angle of attack in Fig.15, it can be observed that as the angle of attack increases, the vehicle's pitching moment gradually decreases in all three wing folding states. Therefore, under Ma = 0.8 conditions, the vehicle can maintain longitudinal static stability by increasing the wing folding angle and varying the angle of attack. The same conclusion can be drawn based on the difference in static stability margin in Fig.16 and the slope of the pitching moment coefficient curve, which is that when the wing folding angle is smaller, the longitudinal stability is better. As the folding angle increases, the longitudinal static stability decreases.

Similarly, during the transonic (Ma=0.8) phase, the effect of wing folding on the vehicle's directional stability follows a pattern similar to that in the subsonic phase. The three wing folding states progressively increase the restorative moment as the sideslip angle increases, indicating that the vehicle maintains static stability. The downward folding of the outer wing causes a pressure difference between the inner and outer surfaces, resulting in a yawing moment generated by the lateral airflow. Fig.17 illustrates that as the folding angle of the outer wing increases, the yawing moment coefficient grows faster with increasing sideslip angle. This implies a stronger capability for the vehicle to recover from directional disturbances and better directional stability.

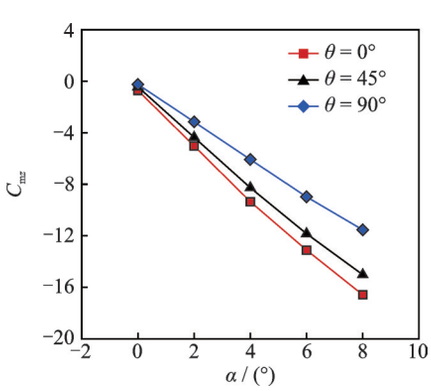

Fig.15 Pitching moment coefficient (H = 5 km, Ma = 0.8, β = 0°)

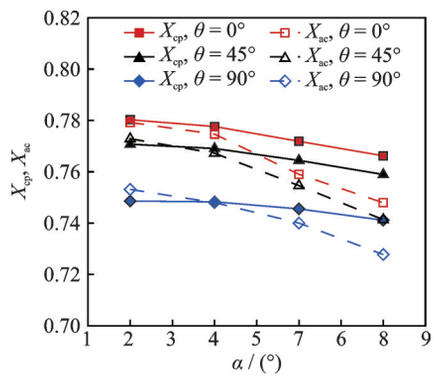

Fig.16 Pressure and aerodynamic center position coefficient (H = 5 km, Ma = 0.8, β = 0°)

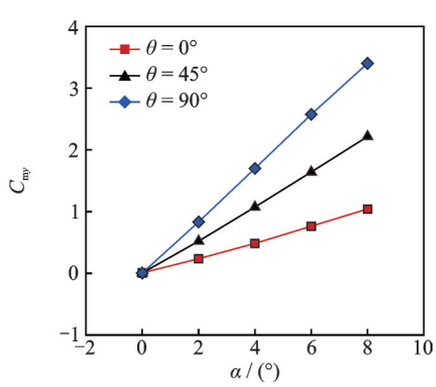

Fig.17 Yawing moment coefficient (H = 5 km, Ma = 0.8, β = 0°)

Fig.18 compares the pressure distribution on the lower surface of the vehicle for two wing folding configurations, 45° and 0°, under the influence of the angle of attack. Both wing folding configurations exhibit a common characteristic where near the leading edge of the wing and the compressed section of the fuselage, there is a high-pressure concentration area at small angles of attack. As the angle of attack

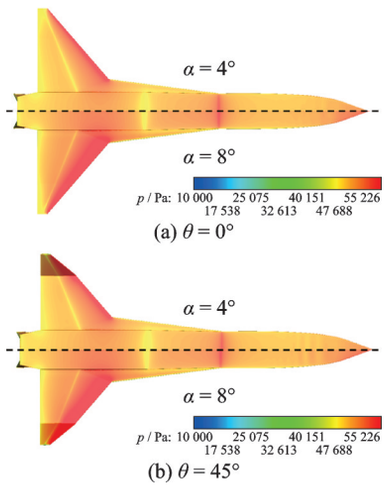

Fig.18 Comparison of pressure distribution on the lower surface at $Ma = 0.8$

increases, the pressure area on the wing's lower surface expands, and the pressure on the lower surface of the fuselage significantly increases. The appearance of a new high-pressure region in the forebody explains the small forward shift of the center of pressure observed in Fig.18. As the angle of attack increases, the relative position relationship of different folding angles remains unchanged. Smaller folding angles result in the center of pressure and focus being located further forward[18].

3.4 Supersonic-speed aerodynamic characteristics analysis

In the supersonic phase, numerical simulation research was conducted under flight conditions with a Mach number of 2. Fig.19 illustrates the lift and drag characteristics of the vehicle in the three different wing folding angle states.

Fig.19(a) depicts the lift coefficient curves for the three different wing folding angle states at supersonic speeds (Ma=2). It can be observed that the lift increases with the angle of attack. There is little difference between the 45° and 0° folding angle states, both of which are higher than the 90° deflection angle state. When flying at $Ma = 2$, lift generation primarily relies on airflow compression on the windward side and expansion on the leeward side. Fig.20 presents the pressure distribution of the axial section of the wing and the symmetry plane to visualize the effect of wing folding on the surrounding flow field.

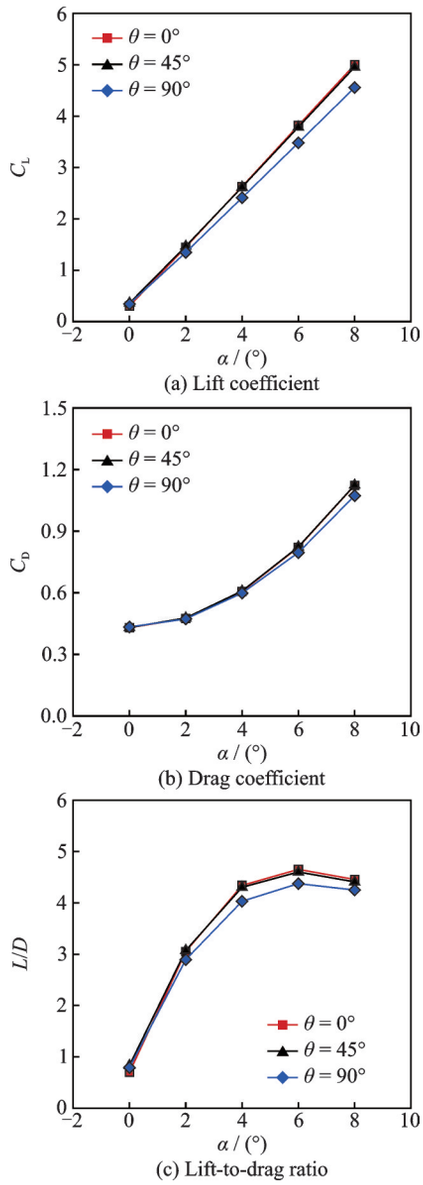

Fig.19 Variation of lift and drag characteristics with angle of attack ($H = 15$ km, $Ma = 2$, $\beta = 0°$)

When the folding angle changes from 0° to 45°, the high-pressure airflow overflowing from the wing's lower surface moves away from the upper surface, resulting in a significant reduction in the low-pressure region compared to the 0° folding angle. At the same time, the downward folding of the wing suppresses the outward leakage of high-pressure airflow from the lower surface, expanding the area of the high-pressure region on the lower surface of the wing, thus exhibiting a similar wave-riding effect[19].

When the wing folding angle reaches 90°, the pressure difference between the upper and lower surfaces of the wing is converted into the pressure dif-

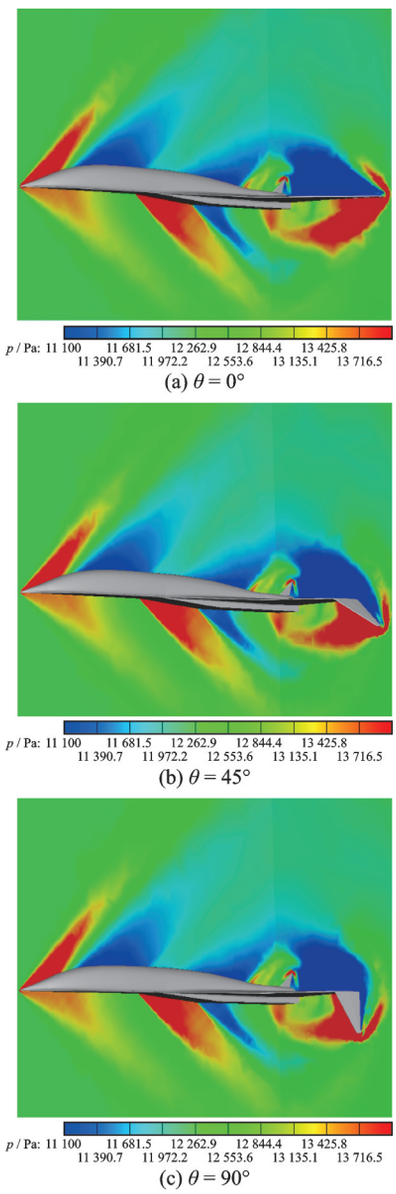

Fig.20 Contour of pressure distribution at symmetry plane and $x = 11.9$ m slice ($Ma = 2$, $\alpha = 4°$)

ference between the inner and outer sides of the vertical wing, which cannot contribute to lift. Therefore, the lift coefficient of the 90° folding angle configuration is smaller than the other two configurations.

The drag experienced by the vehicle under supersonic conditions mainly comes from shock waves, and the influence of the fuselage on the drag is more significant compared to the low-speed state[20]. It can also be seen from the symmetry plane that the folding of the wing does not significantly affect the flow around the fuselage because it is far away from the outer wing. From Fig.19(b), which depicts the variation of the drag coefficient with the angle of attack, it can be observed that the drag coefficient increases as the angle of attack increases for all three-wing folding configurations. However, when the wing is folded at a 90° angle, the effective windward area of the vehicle is reduced, resulting in a lower drag coefficient than the other two configurations.

In terms of lift-to-drag ratio, the lift loss still outweighs the drag reduction, resulting in a smaller lift-to-drag ratio as the folding angle increases. However, under supersonic conditions, the difference in lift is no longer solely dependent on the size of the wing's effective lift area. The increased pressure on the lower surface due to wing folding compensates for the lift loss and reduces the difference in the lift-to-drag ratio.

Fig.21 and Fig.22 present the pitching moment coefficient, pressure center, and aerodynamic center with respect to the angle of attack. From the pitching moment coefficient curve, it can be observed that the vehicle's downward pitching moment increases with increasing angle of attack, indicating that all three wing folding configurations of

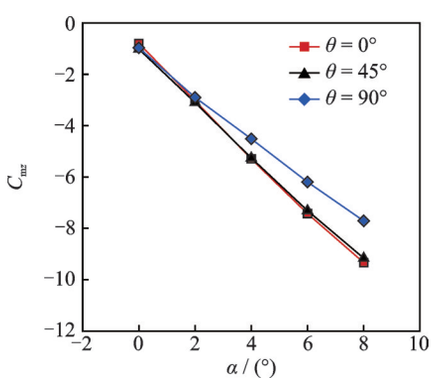

Fig.21 Pitching moment coefficient ($H = 15$ km, $Ma = 2$, $\beta = 0°$)

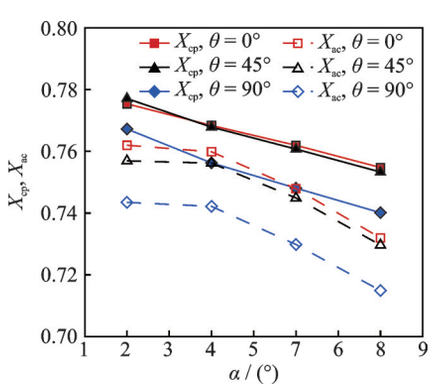

Fig.22 Pressure and aerodynamic center coefficients ($H = 15$ km, $Ma = 2$, $\beta = 0°$)

the vehicle are longitudinally stable.

Looking at the relationship between the positions of the aerodynamic center, it can be noted that a smaller folding angle results in better longitudinal stability. Based on the analysis of lift and drag characteristics, it is known that wing folding restricts the spanwise flow of the airflow over the lower surface of the vehicle, expanding the high-pressure region on the lower surface. However, due to the presence of the folding angle, the folding wing section only provides the longitudinal component of the lifting force when generating the restoring moment. When the folding angle is 90°, and the wing is vertically raised, the outer wing cannot generate an effective longitudinal restoring moment[21]. Therefore, as the folding angle of the vehicle increases, the absolute value of the slope of the pitching moment coefficient with respect to the angle of attack decreases, indicating a decrease in longitudinal stability.

Additionally, due to the changes in the fuselage's forces, the aerodynamic center of the three wing folding configurations moves forward during the supersonic phase compared to the low-speed phase.

Fig.23 shows the variation of the vehicle's yawing moment with sideslip angle. From the curves, it can be observed that as the wing folding angle increases, the vehicle's directional stability improves. When the sideslip angle exceeds 4°, the 0° folding angle configuration becomes directionally unstable. When the wing is in the unfolded configuration, as the sideslip angle increases, the lateral force-acting point continuously moves forward, approaching the center of mass, and cannot generate the required restoring moment. Therefore, as the folding wing's angle increases, the folding wing can enhance the vehicle's directional stability. This phenomenon is more pronounced in the supersonic phase.

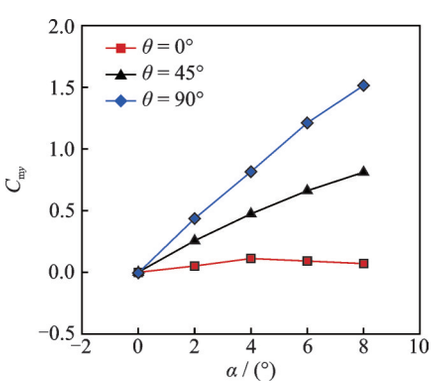

Fig.23 Yawing moment coefficient (H = 15 km, Ma = 2, β = 0°)

3.5 Hypersonic-speed aerodynamic performance analysis

In the hypersonic phase, numerical simulations are conducted under a Mach number of 5. Fig.24 shows the lift coefficient, drag coefficient, and lift-to-drag ratio curves for different folding angle configurations.

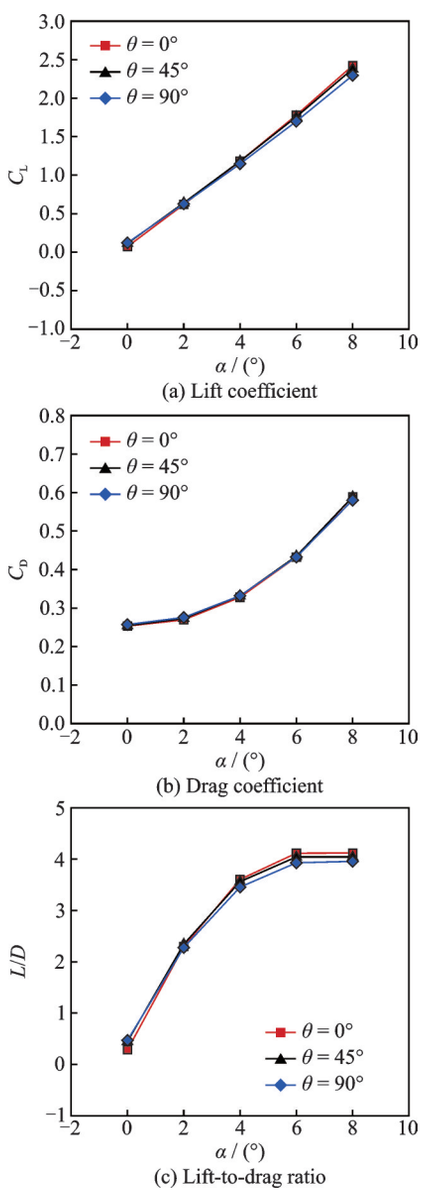

Fig.24 Variation of lift and drag characteristics with angle of attack (H = 24 km, Ma = 5, β = 0°)

From the curves, it can be observed that both the lift coefficient and drag coefficient increase with increasing angle of attack, and there is minimal difference in the aerodynamic performance among the three wing folding configurations. Under subsonic conditions, the maximum difference in lift-to-drag ratio is 1.09; under hypersonic conditions, the maximum difference is reduced to 0.07.

Based on the numerical results, the aerodynamic forces and moment coefficients of the vehicle under hypersonic conditions are not significantly affected by the folding of the wing. Therefore, Fig.25 and Fig.26 are referred to observe the impact of wing folding on the flow field.

Fig.25 shows the pressure distribution in the y=0.01 m plane. It can be observed that as the flight speed increases to a hypersonic state, the shock wave angle at the nose of the vehicle becomes smaller and closer to the body. This downstream extension affects the unfolding section near the wing root, resulting in similar effects of the shock wave at the wing's leading edge for all three folding configurations. The windward state and the force distribution on the wing folding section's upper and lower (or inner and outer) surfaces may vary, necessitating further investigation of the pressure distribution on the wing surface. Analyzing the changes in the flow field and their impact on performance caused by wing folding can be done by studying the pressure distribution on the wing surface.

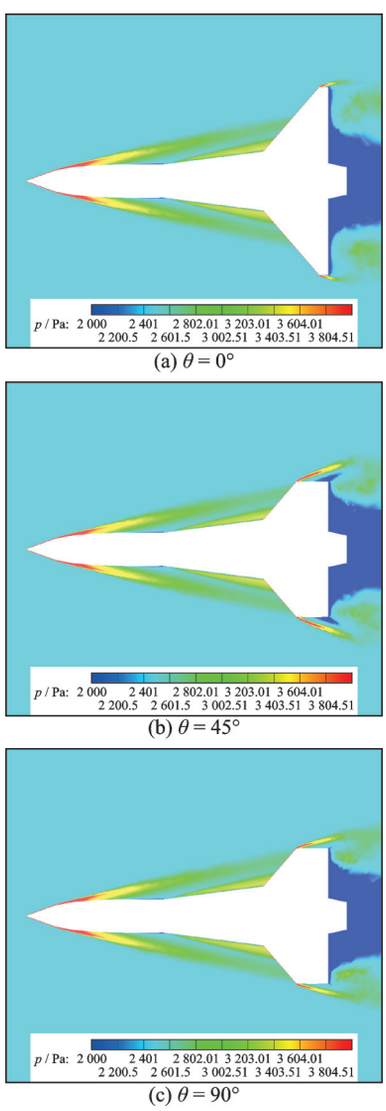

Fig.25 Contour of pressure distribution at y = 0.01 m slice (Ma = 5, α = 4°)

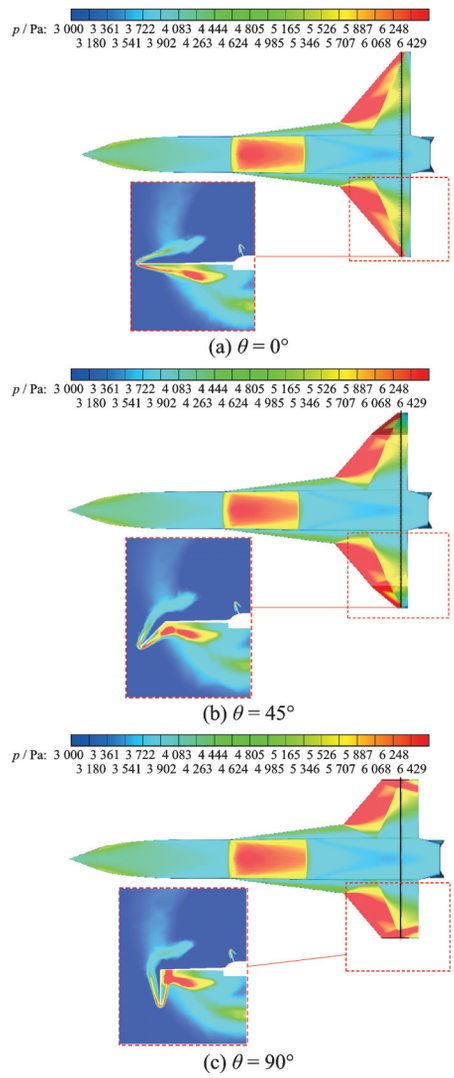

Fig.26 Contour of pressure distribution on the lower surface and around wing (Ma = 5, α = 4°)

In the numerical simulation results under supersonic conditions, it is concluded that wing folding

can restrict the spanwise flow of high-pressure airflow on the lower surface and enhance the compression of the airflow on the lower surface. Therefore, the pressure difference between the upper and lower surfaces of the wing increases as the folding angle increases. This phenomenon becomes more pronounced when the flight speed grows to a hypersonic state (Ma=5). The accumulation of high-pressure airflow on the lower surface significantly affects the pressure distribution on the vehicle surface. Fig.26 illustrates the pressure distribution on the lower surface of the vehicle in different folding states. The main differences appear on the lower surface and inner side of the outer wing. Based on the surface pressure distribution and the flow field distribution around the wing, it can be observed that when the folding angle is small, the high-pressure region on the lower surface is distributed uniformly. As the folding angle increases, the range of the high-pressure area on the lower surface becomes smaller but more concentrated.

Additionally, the pressure difference between the upper and lower surfaces, particularly in the region affected by folding, becomes more extensive. Therefore, during the wing folding process, although the effective windward area of the vehicle is reduced, there is no significant change in the lift and drag coefficients of the vehicle[22]. Until the wing folding angle reaches 90°, with the outer wing being vertically upright, the pressure difference between the upper and lower surfaces of the outer wing is converted into a pressure difference between the inner and outer sides, unable to provide lift. The vehicle's lift coefficient and lift-to-drag ratio are slightly smaller in this state than in the 0° and 45° folding states.

Fig.27 and Fig.28 illustrate the variation of the pitch moment, center of pressure, and aerodynamic center positions with angle of attack in hypersonic conditions. Based on the numerical results, it can be concluded that the vehicle is longitudinally stable in all three folding angle states. As the Mach number increases, the forces acting on the fuselage cause a forward shift in the position of the aerodynamic center. However, the relative positions of the aerodynamic centers remain unchanged among the three wing folding states. The configuration with a smaller folding angle has better longitudinal stability. The differences in longitudinal stability between different folding angles initially decrease and then increase compared to the subsonic, transonic, and supersonic conditions mentioned earlier. The static stability margins change from 1∶0.95∶0.84 to 1∶0.98∶0.88 and then to 1∶0.89∶0.79.

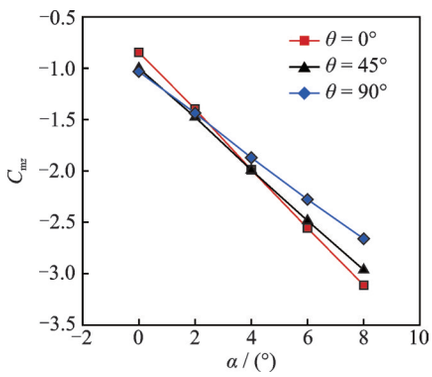

Fig.27 Pitching moment coefficient (H = 24 km, Ma = 5, β = 0°)

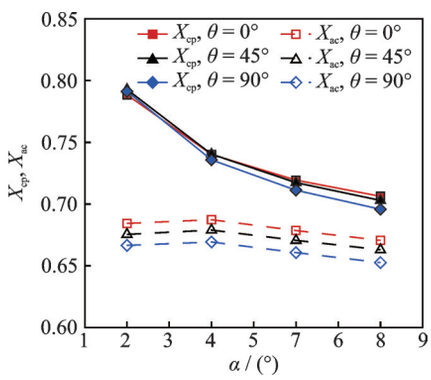

Fig.28 Pressure and aerodynamic center coefficient (H = 24 km, Ma = 5, β = 0°)

Fig.29 presents the variation of the yawing moment with sideslip angle under the hypersonic conditions. The curves show that for folding angles of 0° and 45°, the yawing moment decreases as the sideslip angle increases. Conversely, for a folding angle of 90°, the yawing moment increases with increasing sideslip angle. During the hypersonic phase, wing folding has a more pronounced effect on the vehicle's directional stability. When the folding angle is small, the vehicle is directionally unstable. As the folding angle increases, the influence of the incoming flow on the outer wing generates a restoring moment. Thus, wing folding significantly enhances the

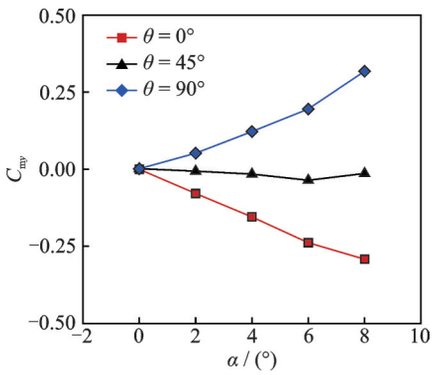

Fig.29 Yawing moment coefficient (H=24 km, Ma=5, $\beta=0°$)

vehicle's directional stability[23].

4 Conclusions

This article initially establishes the aerodynamic configuration of a hypersonic morphing vehicle, focusing on the wing folding morphing scheme as the research subject. The research compares the aerodynamic characteristics, including lift, drag, and static stability, of three different wing folding configurations under various flight conditions[24]. Based on numerical and flow field results, the reasons behind the observed differences are analyzed. The following conclusions are drawn regarding the impact of wing folding on the performance of the hypersonic morphing vehicle.

(1) Lift and drag characteristics: Under the exact flight conditions, the vehicle exhibits a higher lift coefficient, drag coefficient, and lift-to-drag ratio when the wing folding angle is smaller. A smaller wing folding angle at low-speed flight conditions results in a larger wing windward area, leading to a higher lift-to-drag ratio and significant lift advantages, although accompanied by increased drag. As the flight speed increases, the lift mechanism changes, and the compressive effect of the folding outer wing on the lower surface high-pressure airflow becomes more prominent. A larger folding angle leads to a higher pressure differential between the upper and lower surfaces, gradually reducing the difference in lift-to-drag ratio compared to cases with smaller folding angles.

(2) Longitudinal static stability: Under the exact flight conditions, larger wing folding angles result in a forward shift in the aerodynamic center position and a smaller longitudinal static stability margin. However, the aerodynamic center always remains behind the center of mass, and the vehicle maintains longitudinal static stability throughout a wide range of speeds. During the transition from subsonic to hypersonic flight speeds, the changes in forces on the fuselage and wings cause the aerodynamic center to shift rearward and forward. However, the relative position relationship remains unchanged, and the law of better longitudinal stability with smaller folding angles remains valid within the Mach number of 0.3—5. The differences in longitudinal static stability between different wing folding angles initially decrease and then increase.

(3) Directional static stability: The vehicle exhibits better directional stability under the exact flight conditions as the wing folding angle increases. The downward folding of the outer wing compensates for the stabilizer's function, limiting the forward shift of the lateral pressure center and providing a restoring moment. As the flight speed increases, the states with wing folding angles of 0° and 45° gradually transition from directional stability to instability. The state with a 90° folding angle consistently maintains directional stability. With higher flight speeds, the differences in directional stability become more pronounced.

A comprehensive understanding of the advantages and limitations of different wing folding configurations in different flight phases is achieved by comparing the performance differences under various flight conditions. The ability to adjust flight performance based on flight conditions and task requirements has been validated by applying aerodynamic configuration morphing design within a wide-speed range background[25]. The wing folding can be tailored to increase lift or reduce drag based on different flight phases, and the static stability margin can be adjusted for cruising or maneuvering tasks[26]. In conclusion, based on the existing research results, it is possible to carry out more detailed designs of morphing schemes, incorporate flight profiles to form morphing strategies, and provide a theoretical foundation for achieving optimal flight performance in different phases of vehicle operation.

References

[1] DONG Pengcheng, HAN Yuqi, LIU Jinchao. Development analysis of wide adaptability hypersonic aerospace power technology[J]. Aerospace Power, 2020(6): 25-30. (in Chinese)

[2] CHENG Zhaobin, LIAO Menghao, LI Fei, et al. Analysis of aerodynamic layout design characteristics of hypersonic vehicle[J]. Aeronautical Science & Technology, 2022,33(2): 6-11. (in Chinese)

[3] DONG Yanfei, CHEN Yuankai, PENG Jinjing. Development and the prospect of variable swept wing technology[J]. Flight Dynamics, 2014, 32(2): 97-100. (in Chinese)

[4] DAI P, YAN B B, PANG M H, et al. Design and aerodynamic performance analysis of a variable-sweep-wing morphing waverider[J]. Aerospace Science and Technology, 2020, 98: 105703.

[5] JIAO Zihan, FU Qiujun, DENG Fan, et al. Aerodynamic design and experimental study of full-speed intelligent deformable vehicle[J]. Journal of Solid Rocket Technology, 2017, 40(5): 653-659. (in Chinese)

[6] BAI Peng, CHEN Qian, XU Guowu, et al. Development status and prospect of key technologies of intelligent deformable vehicle[J]. Acta Aerodynamica Sinica, 2019, 37(3): 426-443. (in Chinese)

[7] XU Guowu, BAI Peng, CHEN Bingyan. Analysis of lift-drag characteristics of a new concept of intelligent morphing vehicle[J]. Chinese Quarterly of Mechanics, 2013, 34(3): 444-450. (in Chinese)

[8] LIN Peng, ZUO Linxuan, WANG Xiao, et al. Discussion on vehicle/engine integration technology of future combat vehicle[J]. Aerospace Power, 2018(2): 52-57. (in Chinese)

[9] XIAO Ling. Dynamic equivalent method and aeroelastic study of folding wing tip[D]. Dalian: Dalian University of Technology, 2021. (in Chinese)

[10] LI Xiankai, WANG Xiao, LIU Jun, et al. Study on aerodynamic layout technology of horizontal takeoff and landing hypersonic vehicle[J]. Aeronautical Science & Technology, 2020,31(11): 7-13. (in Chinese)

[11] GUO Shuzhen, ZHENG Xiangming, YIN Chong, et al. Aerodynamic characteristics analysis of folding wing vehicle[J]. Advances in Aeronautical Science and Engineering, 2013,4(3): 358-363. (in Chinese)

[12] WANG Zaiduo, WANG Hui, DING Nan, et al. Development of hypersonic vehicle technology[J]. Science & Technology Review, 2021, 39(11): 59-67. (in Chinese)

[13] LUO S B, SUN Y H, LIU J, et al. Performance analysis of the hypersonic vehicle with dorsal and ventral intake[J]. Aerospace Science and Technology, 2022, 131: 107964.

[14] LUO S B, SUN Y H, LIU J, et al. Basic static stability and control characteristics of hypersonic vehicles with dorsal and ventral intake[J]. Aerospace Science and Technology, 2023, 134: 108159.

[15] DING Feng. Research of a novel airframe/inlet integrated full-waverider aerodynamic design method-ology for air-breathing hypersonic vehicles[D]. Changsha: National University of Defense Technology, 2016. (in Chinese)

[16] DING Yulin, HAN Zhonghua, QIAO Jianling, et al. Progress in key technologies of overall aerodynamic layout design of ultrasonic civil vehicle[J]. Acta Aeronautica et Astronautica Sinic, 2023, 44(2): 20-46.

[17] LIANG Haichao, ZENG Jinyuan, CHEN Qian, et al. Aerodynamic characteristics of trailing edge airfoil with a continuous smooth deflection in transonic cruise state[J]. Aeronautical Science & Technology, 2021, 32(5): 7-16. (in Chinese)

[18] YANG Guang, ZHAO Hongxin, QIN Jiacheng, et al. Study on aerodynamic characteristics of oblique flying wing layout[C]//Proceedings of the 9th China Aviation Society Youth Science and Technology Forum. Xi'an, China: Chinese Society of Aeronautics and Astronautics,2020. (in Chinese)

[19] GOODMAN J L. History of space shuttle rendezvous and proximity operations[J]. Journal of Spacecraft & Rockets, 2006, 43(5): 944-959.

[20] YUAN Jisen, SUN Jue, LI Lingyu, et al. Development of laminar flow layout design and evaluation technology for supersonic vehicle[J]. Acta Aeronautica et Astronautica Sinica, 2022, 43(11): 63-98. (in Chinese)

[21] ZHANG Yufei, QI Zheng, TIAN Shichao, et al. Aerodynamic layout design of reusable hypersonic vehicle[C]//Proceedings of the Abstracts of Papers of the 11th National Symposium on Fluid Mechanics. Beijing, China: The Chinese Society of Theoretical and Applied Mechanics, 2020. (in Chinese)

[22] LYU Dailong, CHEN Shaosong, XU Yihang, et al. Aerodynamic characteristics of close-range coupled canard missile[J]. Acta Armamentarium, 2022, 43(6): 1316-1325. (in Chinese)

[23] GLASS J B, GLASS Z S, MACKOWSKI A, et al. Design and analysis of a single-stage hypersonic concept for ultra-rapid global travel[C]//Proceedings of

the 15th AIAA International Space Planes and Hypersonic Systems and Technologies Conference. Dayton, Ohio, America: American Institute of Aeronautics and Astronautics, 2008.

[24] ZHANG Dengcheng, LUO Hao, ZHANG Yanhua, et al. Study on aerodynamic characteristics of hypersonic vehicle with wide velocity range and variable configuration[J]. Journal of Solid Rocket Technology, 2019, 42(1): 128-134. (in Chinese)

[25] ZUO Linxuan, YOU Ming. Research on aerodynamic configuration, stability and control characteristics of hypersonic vehicle[J]. Aeronautical Science & Technology, 2020, 31(11): 47-53. (in Chinese)

[26] LUO Shibin. Airframe/engine integrated design of hypersonic vehicle[M]. Beijing: Science Press, 2018. (in Chinese)

Acknowledgements This work was supported by the foundation of National Key Laboratory of Science and Technology on Aerodynamic Design and Research (No. 614220121020114) and the Key R&D Projects of Hunan Province (Nos.2021GK2011, 2023GK2022).

Authors Prof. **LUO Shibin** obtained his Ph. D. degree aerospace science and technology from the Department of Aerospace Science and Engineering, National University of Defense Technology, in 2004. From 2004 to 2015, he worked as an associate professor at the National University of Defense Technology. He won the second prize of the National Science and Technology Progress Award in 2014. He joined Central South University in 2016 and he is currently a professor of Research institute of Aerospace Technology. His research focuses on hypersonic vehicle design.

Dr. **LIU Jun** obtained his Ph.D. degree fluid mechanics from the School of Aeronautics, Northwestern Polytechnical University, in 2015. He joined Central South University in 2015 and he is currently an associate professor of Research Institute of Aerospace Technology. His research focuses on aerodynamic configuration design of aerospace vehicle and aerodynamic optimization design.

Mr. **YUE Hang** received his M.S. degree in Aerospace science and technology from the Research institute of Aerospace Technology, Central South University, in 2023. His research focuses on the aerodynamic configuration design of hypersonic vehicles.

Author contributions Prof. **LUO Shibin** planned the research content and guided the numerical simulation research. Mr. **YUE Hang** carried out the numerical simulation research and wrote the manuscript. Dr. **LIU Jun** contributed to the analysis of the results and manuscript writing. Dr. **SONG Jiawen** contributed to the data processing. Dr. **CAO Wenbin** provided the code for CFD numerical simulation. All authors commented on the manuscript draft and approved the submission.

Competing interests The authors declare no competing interests.

(Production Editor: SUN Jing)

高超声速变体飞行器宽速域气动特性研究

罗世彬，岳　航，刘　俊，宋佳文，曹文斌

（中南大学航天技术研究院，长沙 410083，中国）

摘要：宽速域飞行是高超声速飞行器的重要设计目标和发展方向。然而，复杂的环境变化给固定外形飞行器在不同飞行条件下的气动布局设计带来了矛盾。高超声速变体飞行器可以通过呈现不同的构型来适应各种飞行条件并满足性能要求。本文通过数值模拟的方法来研究折叠翼高超声速飞行器的气动性能。研究重点是在不同飞行高度和马赫数下，探究不同机翼折叠状态对应气动布局的升阻比、纵向静稳定性和航向静稳定性。比较了不同机翼折叠角度(0°、45°、90°)对气动性能的影响。结果表明，在所研究的整个速度范围内(Ma=0～5)，较小的机翼折叠角会导致较高的升力系数、阻力系数和升阻比。机翼折叠角为0°时，升阻比最高。在纵向稳定性方面，折叠角度较小的布局具有更好的纵向稳定性。随着马赫数的增加，不同折叠角度之间的纵向稳定性差异最初减小，然后增大。静态稳定裕度从1∶0.95∶0.84变为1∶0.98∶0.88，后变为1∶0.89∶0.79。此外，具有较大机翼折叠角的构型表现出更好的航向稳定性。所有3种机翼折叠布局状态在低速飞行阶段都是航向静稳定的。随着马赫数的增加，0°和45°折叠角逐渐变得航向静不稳定。

关键词：宽速域；变体飞行器；折叠翼；气动性能；高超声速飞行器